Environmental Technology & Innovation 28 (2022) 102640

Contents lists available at ScienceDirect

Environmental Technology & Innovation

journal homepage: www.elsevier.com/locate/eti

Removal of Cu, Pb and Zn from stormwater using an industrially manufactured sawdust and paddy husk derived biochar

Pamodithya Wijeyawardana [a,b], Nadeeshani Nanayakkara [b], Chamila Gunasekara [a], Anurudda Karunarathna [c], David Law [a], Biplob Kumar Pramanik [a,d,*]

[a] School of Engineering, RMIT University Melbourne, Australia
[b] Faculty of Engineering, University of Peradeniya, Sri Lanka
[c] Faculty of Agriculture, University of Peradeniya, Sri Lanka
[d] Water: Effective Technologies and Tools (WETT) Research Centre, RMIT University, Australia

ARTICLE INFO

Article history:
Received 31 March 2022
Received in revised form 26 April 2022
Accepted 28 April 2022
Available online 6 May 2022

Keywords:
Industrial biochar
Sawdust
Paddy husk
Heavy metals
Stormwater

ABSTRACT

Direct flow of untreated stormwater containing Cu, Pb and Zn is of immediate concern to aquatic life in waterways. To date, most biochar used has been synthesized under controlled laboratory conditions using furnaces purged with inert gasses. In this study, the removal of Cu, Pb and Zn using biochar synthesized using paddy husk and sawdust feedstocks has used an industrial scale double chamber downdraft pyrolysis reactor. The effect of pyrolysis temperature and the effect of feedstock in the removal of Cu, Pb and Zn was evaluated by conducting batch adsorption experiments. Synthesized adsorbent materials were characterized using proximate analysis, zero-point charge, scanning electron microscopy, X-ray diffraction and Fourier Transform infrared spectroscopy. The biochar yield was in a lower range compared with the literature attributed to the higher heating rate (50 °C/min) in the pyrolizer. Maximum removal efficiencies were observed when the initial pH was at the value closest, when below the solubility limit for the heavy metals. The paddy husk biochar and sawdust biochar synthesized in the temperature range 350–450 °C and 450–550 °C performed best in the removal of the three heavy metals. Chemisorption was the main mechanism for the removal of the three heavy metals. The maximum adsorption capacities of Cu and Zn were 10.27 and 6.48 mg/g was achieved with paddy husk biochar and a maximum Pb adsorption capacity of 17.57 mg/g was achieved by sawdust biochar. Surface complexation, co-precipitation, p-electron interactions, physical adsorption and surface precipitation were the main mechanisms of removal of the three heavy metals.

1. Introduction

The pollutants collected on impervious surfaces are washed off by stormwater runoff and are conveyed to receiving waterways. Due to the conveyance of pollutants by stormwater, water sources become severely polluted (Wang and Liu, 2017). Therefore, stormwater has been identified as a major source of non-point source pollutants, especially in the urban

* Corresponding author at: School of Engineering, RMIT University Melbourne, Australia.
E-mail address: biplob.pramanik@rmit.edu.au (B.K. Pramanik).

https://doi.org/10.1016/j.eti.2022.102640

environment (Zuraini et al., 2018; Sidhu et al., 2020). Due to the toxicity, non-degradability and bioaccumulation, heavy metals are considered one of the most critical pollutants present in stormwater runoff (Ma et al., 2016; Sidhu et al., 2020). Although some heavy metals are essential micronutrients for life, they can cause severe poisoning (Saleh, 2015; Alhashimi and Aktas, 2017). When animals and plants are exposed to water and soil contaminated with heavy metals, the metals collect in their tissues (Duruibe et al., 2007; Tchounwou et al., 2012). If ingested, the heavy metals are acidified in the stomach and oxidized into their oxidative states which are more toxic than the unoxidized states of the heavy metals (Engwa et al., 2018; Wijeyawardana et al., 2022). Although the direct risk to humans by single heavy metals in urban stormwater is not significant due to their low concentrations, it is an immediate concern to the aquatic life in the receiving waters (Ma et al., 2016). Therefore, recent studies have focused on treating urban stormwater to meet water quality objectives for reuse and/or safe discharge to an open water environment (Mullaney and Lucke, 2014). Past studies have observed significant concentrations of Cu, Cd, Cr, Ni, and Zn in stormwater (Reddy et al., 2014). However, the most common heavy metals found in stormwater are Cu, Pb and Zn (Sakson et al., 2018; Wijeyawardana et al., 2022). The quality of stormwater degrades due to the strong mobility and toxicity of Cu, Pb and Zn (Ma et al., 2016; Chen et al., 2020). Furthermore, Cu and Zn have been identified as the primary cause of toxicity in stormwater and are identified as priority pollutants by the USEPA (Kayhanian et al., 2008; USEPA, 2014). Bioaccumulation of Cu ions in humans causes harm to the brain, heart, skin and pancreas (Park et al., 2017). Pb toxicity can lead to kidney failure, damage to the nervous system and impair muscle function (Efome et al., 2018a,b,c; Gu et al., 2021). Excess amounts of Zn cause stomachache, dehydration, nausea, dizziness, and electrolyte imbalance (Park et al., 2017)

Adsorption, filtration, ion exchange, and redox reactions have been used to treat heavy metals in previous studies (Batool et al., 2017). However, adsorption is considered versatile, cheap and easy for large-scale heavy metal treatment (Batool et al., 2017; Efome et al., 2018b). Biochar is a carbon-rich solid obtained via thermal degradation of biomass in an oxygen-limited environment (Inyang et al., 2015; Shen et al., 2017). Biochar has unique properties including specific surface area, porous structure, and surface functional groups which makes it a good adsorbent (Dai et al., 2019; Sun et al., 2019). Of the two types of pyrolysis processes: fast and slow, the use of slow pyrolysis is more common than fast pyrolysis when biochar is the primary focus of the study (Tomczyk et al., 2020). Properties of biochar primarily depend upon the feedstock and the pyrolysis temperature (Tan et al., 2015; Dai et al., 2019). The general temperature range used for biochar synthesis is between 350–750 °C. Lower pyrolysis temperatures usually preserve the oxygen-containing functional groups which induce the Cation Exchange Capacity (CEC) of biochar (Lago et al., 2021). On the other hand, increasing the pyrolysis temperature reduces these groups which decrease the CEC of biochar. Contrary to the behavior of CEC, the surface area of the biochar increases with increasing pyrolysis temperatures. Biochar synthesized from materials such as algae, tobacco stems, hardwood, softwood, rice husks, and straw has been used successfully in the past for the removal of Cu, Pb and Zn (Poo et al., 2018; Zhou et al., 2018; Zhao et al., 2020). Biochar was synthesized with a mix of hardwoods, which achieved approximately 58% and 70% removal of Cu and Zn respectively (Chen et al., 2011). Above 95% Cu removal efficiency had been observed using farmyard manure, poultry manure-derived biochar and wasted marine macro-algae (Batool et al., 2017; Poo et al., 2018). Additionally, the environmental impacts of using biochar as a functional unit for the adsorption of heavy metals are lower than that of activated carbon (Shen et al., 2017).

Agricultural biomass is one of the most abundant renewable resources with the capacity to be turned into biochar (Dai et al., 2019). The usage of agricultural waste materials in biochar synthesis helps to reduce the cost of biochar production (Tan et al., 2015). This is mainly due to the abundance of the material in large quantities and the materials being considered as a waste requiring disposal. Paddy husk also referred to as rice husk, is the by-product of the rice milling industry which comprises 20% w/w of the total paddy products (Kumar et al., 2021). Sawdust is also a similar feedstock material that can be turned into biochar and is available in huge quantities (Kumar et al., 2021). However, most biochar used in heavy metal removal in reported literature is prepared in controlled laboratory settings where muffle furnaces purged with inert gases are used (Zhao et al., 2020; Mbui et al., 2021; Yankovych et al., 2021). This is a high energy-intensive process, and only a very limited quantity of biochar can be produced. Additionally, according to European guidelines the pyrolytic gases produced during the pyrolysis process should be burned to supply energy to the pyrolysis process (Heredia Salgado et al., 2020).

Comparatively, the use of an industrial type of biochar plant helps in producing high quantities of cleaner biochar, with lower emissions of carbon monoxide, hydrocarbons, and fine particles and has lower greenhouse gas emissions (Dai et al., 2019). However, there is very limited research on the use of industrially manufactured biochar in the removal of heavy metals. Furthermore, the use of vertical moving bed-type pyrolysis reactors for biochar production is limited (Soni and Karmee, 2020). Hence, this research evaluates the effectiveness of biochar, synthesized in a double chamber draft down type of pyrolysis reactor, utilized for the removal of Cu, Pb and Zn. This reactor does not use any inert gas during operation, neither diesel nor natural gas for the heating process. The pyrolytic gases are burnt to supplement the energy requirement for pyrolysis as well. Further, the effect of initial pH, adsorbent dosage and contact time on the removal efficiencies of Cu, Pb and Zn are studied. A range of characterization techniques such as Scanning Electron Microscopy (SEM) with Energy Dispersive X-Ray Analysis (EDX), Fourier transform infrared spectroscopy (FTIR), and X-ray diffraction analysis (XRD) are used to characterize the synthesized biochar and to identify the main mechanisms of removal of Cu, Pb and Zn using the synthesized biochar.

2. Materials and methods

2.1. Reagents

Stock solutions of Cu, Pb and Zn with a concentration of 1000 mg/L were prepared by using copper (II) nitrate Cu $(NO_3)_2{\cdot}3H_2O$ (Sigma Aldrich, USA), lead (II) nitrate, Pb $(NO_3)_2$ (Sigma Aldrich, USA) and zinc (II) nitrate, Zn $(NO_3)_2{\cdot}6H_2O$ (Sigma Aldrich, USA) with assay above 99% and distilled water. All adsorption tests were done using synthetic stormwater. For each adsorption experiment, fresh solutions of 10 mg/L of each heavy metal were used by diluting stock solutions with distilled water. 1 M HCl solution was made by diluting concentrated (37%) hydrochloric acid (Sigma Aldrich, USA) with distilled water. 1 M NaOH solution was prepared by dissolving NaOH pellets (Daejung, Korea) with an assay of 97% in distilled water. HNO_3(Sigma Aldrich, USA) with 70% assay was used for acidifying the filtered samples.

2.2. Biochar synthesis

A continuous type Down Draft Double Chamber slow pyrolysis reactor shown in figure S1, developed by Alahakoon et al. (2018) was used for the biochar synthesis using paddy husk and mixed wood sawdust as feedstocks. The biochar output rate was around 1.0 kg per hour. Coconut shells were used as the primary fuel to supply heat to the pyrolysis chamber. The syngas generated from the pyrolysis process was directed to the heating chamber via a recirculation system. Thus, syngas was used as a supplementary fuel to supply heat to the pyrolysis chamber.

The Sawdust was sieved with a 4 mm sieve to remove impurities (e.g., larger wood particles) that might clog the pyrolysis chamber. As paddy husk is uniformly graded compared to sawdust, no sieving was required before pyrolysis. Six sets of biochar were made adhering to three temperature ranges: 350–450 °C, 450–550 °C and 550–650 °C with a residence time of 25 ± 5 min. Following pyrolysis, the biochar was quenched with water to cool it to room temperature (20 ± 2 °C). The biochar was then oven-dried for 24 h and sieved from a 2 mm sieve before storing in airtight containers. The biochar materials synthesized at 350–450 °C, 450–550 °C and 550–650 °C using Paddy husk Biochar (PHBC) are abbreviated as PHBC1, PHBC2 and PHBC3. The biochar materials synthesized using Saw Dust Biochar (SDBC) adhering to the respective temperature ranges are abbreviated as SDBC1, SDBC2 and SDBC3.

2.3. Adsorption tests

2.3.1. Effect of initial pH

The initial pH of synthetic Cu, Pb and Zn solutions was adjusted by adding 1 M hydrochloric acid or 1 M sodium hydroxide as required. All adsorption experiments were carried out in High-Density Polyethylene (HDPE) Vessels (500 ml) at a temperature of 25 ± 1.0 °C. The samples were placed in a thermostatic reciprocating shaker set to 150 rpm for a specified time (24 h). After the adsorption experiments were completed, the supernatant was filtered using 0.45 μm filter papers and acidified with HNO_3 before final metal concentrations were determined.

To evaluate the effect of initial pH, 1500 ml of 10 mg/L synthetic heavy metal solution was prepared in a borosilicate vessel and the pH was adjusted to the desired value (pH 3–9). Once the specified pH had been achieved, 100 ml of solution was measured and transferred to a High-Density Polyethylene Vessel and a dosage (1 g/L) of adsorbent was added. The adsorption test was conducted over a 24 h period. The removal efficiencies were calculated using Eq. (1). *Ci* and *Ce* (mg L^{-1}) represent the initial and equilibrium concentration of the heavy metal, respectively.

$$\text{Removal efficiency} = \frac{(Ci - Ce)}{Ci} \times 100\% \tag{1}$$

2.3.2. Adsorption kinetics

The effect of contact time on the adsorption of heavy metals at the optimum pH was studied to model the adsorption kinetics. 100 mL of each pollutant were placed in HDPE bottles and adsorbent quantities equal to 1 mg L^{-1} were added. The samples were then placed in a thermostatic reciprocator for specified time intervals ranging from 5 min to 24 h. After the test, the residual metal concentration was determined, and the respective adsorption capacities were calculated.

Pseudo-first-order and pseudo-second-order models were used to examine the adsorption kinetics of Cu, Pb and Zn removal. The linearized model equations are given in Eq. (2) and Eq. (3). Pseudo-first-order model

$$\ln(q_e - q_t) = \ln q_e - K_1 t \tag{2}$$

Pseudo-second-order model

$$\frac{t}{q_t} = \frac{1}{K_1 (q_e)^2} + \frac{1}{q_e} \tag{3}$$

here q_t is the amount of sorbate adsorbed at time t (minutes) (mg g^{-1}); k_1 is the equilibrium rate constant of the pseudo-first-order model (h^{-1}); k_2 is the equilibrium rate constant of PSO adsorption (g mg^{-1} h^{-1}).

2.3.3. Adsorption isotherms

Adsorbent dosages ranging from 0.125 g/L to 2 g/L were used for the isotherm analysis. 100 mL of respective synthetic heavy metal solution was put in a HDPE bottle and adsorbents corresponding to the selected adsorbent dosages were added. Adsorption tests were conducted for the respective equilibrium times determined through the kinetics analysis. The respective adsorption capacities were calculated by comparing the residual heavy metal concentration with the initial heavy metal concentration.

Both Freundlich and Langmuir models were used to describe the adsorption isotherms. The model equations for the two models are shown in Eq. (4) and Eq. (5).

Freundlich model:

$$\log(q_e) = \log(K) + \frac{1}{n}\log(C_e) \tag{4}$$

Langmuir model:

$$\frac{C_e}{q_e} = \frac{1}{b \cdot Qm} + \frac{C_e}{Qm} \tag{5}$$

Here K is the Freundlich distribution coefficient, indicating adsorption capacity (L/g), $1/n$ is a Freundlich dimensionless parameter, indicating adsorption intensity, Q_m is a Langmuir parameter, that expresses the maximum metal uptake (mg/g), b is a Langmuir parameter, indicating the adsorption energy (L/mg), q_e is the amount of heavy metal adsorbed, per adsorbent mass unit (mg/g), at equilibrium and C_e is the equilibrium heavy metal concentration in the solution (mg/L).

2.4. Analysis methods

The pH values were measured using a pH probe (pH probe; Orion 910003, U.S.A) connected to a multiparameter meter (Thermo Orion A325, USA). The proximate analysis was performed following the ASTM–D1762-84 Standard. Zero-point charge (pH_{zpc}) was measured with the pH drift method (Xu et al., 2021). The surface functional groups were determined by FTIR (UATR two; PerkinElmer, USA). SEM-EDX (EVO 18; ZEISS, Germany) was used to observe the microstructures and element compositions. The mineral compositions of the adsorbents were determined by XRD (Bruker D8 Advance X-ray diffractometer). The concentrations of Cu, Pb and Zn in the solution were measured by an atomic absorption spectrometer (Shimadzu AA-7000, Japan). An elemental analyzer (EA) was used to measure element (C/H/N/O) composition.

3. Results and discussion

Yield, point of zero charge, proximate analysis and SEM-EDX, FTIR analysis were performed on the six biochar materials synthesized using paddy husk and sawdust. The effect of initial pH, contact time and adsorbent dosage on the removal of Cu, Pb and Zn was determined and the FTIR spectra of the spent adsorbents were compared with fresh adsorbents to assess the mechanisms of removal.

3.1. Characterization of biochar

3.1.1. FTIR spectra of biochar

The FTIR spectra qualitatively demonstrate the differences in functional groups present in the biochar due to changes in pyrolysis temperature and feedstock used (Wang and Liu, 2017). Biochar prepared in this study shows a higher number of functional groups in the lower frequency range (<1750 cm^1). This observation is in agreement with previous studies (Lago et al., 2021). Fig. 1(a) and (b) show the FTIR spectra of the feedstocks and synthesized biochar of paddy husk and sawdust respectively. The major peaks of paddy husk biochar are found around 460 cm^{-1}, 796 cm^{-1}, 1088 cm^{-1}, 1566 cm^{-1}, 2098 cm^{-1}, and 3055 cm^{-1}. These correspond to Si–O–Si, aromatic C–H or Si–H or b-ring of pyridine, silanols (Si–OH) and siloxanes (Si–O–Si–OH) groups, stretching of COO–, C=O of ketones and O–H group due to carboxylic acid or water adsorption, respectively (Wang and Liu, 2017; Mbui et al., 2021). The intensity of the peak at 1088 cm^{-1} reduced in 350–450 °C (PHBC1) to 450–550 °C (PHBC2) and then increased at 550–650 °C. However, the intensity of the peak is highest at 350–450 °C. Although a decrease in peak intensity is expected with increasing pyrolysis temperature, this observation could also be due to the high ash content in the 550–650 °C temperature range. The result from the proximate analysis confirms this hypothesis where the ash content of PHBC3 is about 30% higher than that of PHBC2. The same phenomena could account for the increase in the O–H peak found at 3055 cm^{-1}.

The major peaks identified in the sawdust biochar are found around 460 cm^{-1}, 1090 cm^{-1}, 1422 cm^{-1}, 1593 cm^{-1}, 2092 cm^{-1}, and 3400 cm^{-1}. These correspond to Si–O–Si, alcohols (–OH) and C–O groups or siloxanes (Si–O–Si–OH) groups, CO_3^{-2}, aliphatic –C=C–, C=O of aliphatic aldehyde and O–H group (alcoholic and phenolic) (Štefelová et al., 2017; Wang and Liu, 2017; Tomczyk et al., 2020). A decrease in the O–H peak with increasing pyrolysis temperature can be observed especially in SDBC. This observation has also been made in previous studies (Wang and Liu, 2017). A decrease in peak intensity is observed with increasing pyrolysis temperature. This observation is attributed to the lowering of oxygen-containing functional groups with increasing pyrolysis temperature, in agreement with previous studies (Wang and Liu, 2017; Zhou et al., 2018; Mbui et al., 2021).

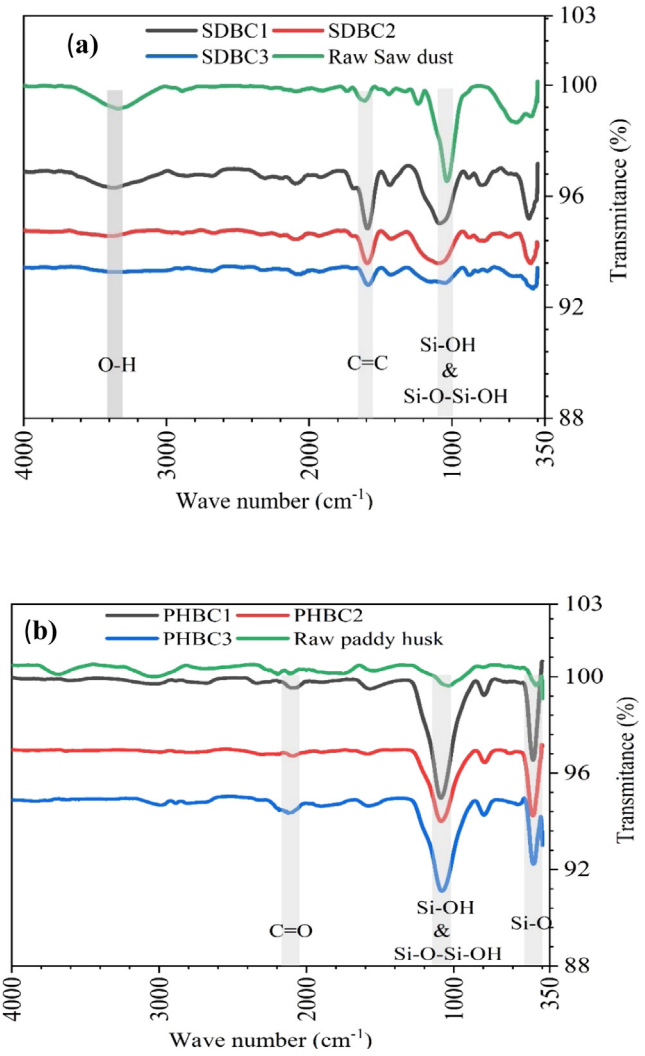

Fig. 1. FTIR spectra of (a) Raw paddy husk and paddy husk biochar; (b) Raw sawdust and sawdust biochar.

3.1.2. Zero-point charge and proximate analysis of feedstock and biochar materials

From the supply of heat during the pyrolysis process, the feedstock is converted to biochar, bio-oil and syngas. The biochar yield values represent the loss of matter as bio-oil and syngas. The yield, zero-point charge and proximate analysis data of the biochar materials are given in Table 1. With the increase in pyrolysis temperature, more bio-oil and syngas are liberated from the feedstock (Dunnigan et al., 2018). Therefore, a lowering of the biochar yield is expected with the increase in pyrolysis temperature due to the formation of more gaseous products (Lin and Kuo, 2012; Dunnigan et al., 2018). A biochar yield of 24%–40% has been observed previously when sawdust is used as the feedstock (Lin and Kuo, 2012; Hodgson et al., 2016; Feola Conz et al., 2017) and when using paddy husk as feedstock a biochar yield of 25%–50% has been observed (Tripathi et al., 2016; Feola Conz et al., 2017; Dunnigan et al., 2018). In this study, the yields range from 23%–27% and 30%–38% for sawdust and paddy husk feedstocks respectively. The results of this study are towards the lower end of yields observed in available literature for both sawdust feedstock. This is attributed to the higher heating rate (50 °C/min) used and the use of an industrial-scale pyrolizer. The increase in the heating rate increases the liquid (bio-oil) and syngas yields which lower the biochar yield (Williams and S, 1996). Comparatively, a heating rate of less than 30 °C/min is used in the cited literature and controlled laboratory conditions are usually used in biochar synthesis. Furthermore, Crombie et al. (2013) observed that the effect of heating rate on SDBC yield is more than the PHBC yield. Thus, the yield of SDBC has reduced more than PHBC compared with values available in the literature.

The point of zero charge (pH_{zpc}) indicates the solution pH in which the surface charge of the adsorbent is neutral. When the pH of the solution is lower than the pH_{zpc}, the surface of the adsorbent is protonated (Zhou et al., 2017), hence, the surface will be positively charged. When the solution pH falls above the pH_{zpc}, the surface of the adsorbent is negatively

Table 1
Variation of pH_{zpc} and proximate analysis data of the raw and biochar materials.

Biochar material	Yield (%)	pH_{zpc}	Moisture content (%)	Ash content (%)	Volatile matter (%)	Fixed matter (%)
Raw sawdust	–	–	10.7	1.3	79.8	18.9
SDBC 1	27.4 ± 1.9	7.6 ± 0.20	2.5	4.3	27.7	68.0
SDBC 2	25.8 ± 2.1	7.80 ± 0.26	1.7	5.7	23.3	71.0
SDBC 3	22.7 ± 2.8	8.10 ± 0.29	1.8	9.2	15.3	75.5
Raw paddy husk	–	–	7.9	21.8	63.9	14.3
PHBC 1	38.1 ± 1.7	8.10 ± 0.27	7.4	41.1	14.4	44.5
PHBC 2	34.4 ± 1.9	8.40 ± 0.38	5.2	48.2	12.2	39.6
PHBC 3	30.5 ± 2.3	8.75 ± 0.24	5.0	55.1	8.5	36.4

charged which favors the attraction of cationic pollutants to the surface of the adsorbent (Zhou et al., 2017; Xu et al., 2021). The relative surface charge of the adsorbents' surface respective to the initial pH of the solution is shown in Figure S2. Although the increment of solution pH decreases the positive charge on the surface, precipitation of heavy metals causes the removal efficiencies to be lower. This is discussed in detail in Section 3.2.1.

The volatile matter filled in the micropores of biochar is released as pyrolysis temperature is increased (Tomczyk et al., 2020). This is due to the cracking of the volatile fraction of the feedstock into liquids and gasses instead of biochar when the temperature increases (Tomczyk et al., 2020). Therefore, a decrease in volatile matter content is expected as the pyrolysis temperature is increased. The results of volatile mater content for PHBC and SDBC show experimental evidence of the lowering of volatiles with increasing pyrolysis temperature. The typical ash content of agricultural feedstocks is 0.3%–8.4% (Dunnigan et al., 2018). However, the ash content of rice husk is high (around 20%) compared to typical agricultural feedstocks due to the presence of high silica content (Dunnigan et al., 2018). Hence, the ash content of PHBC is higher than SDBC. A similar observation was made by Crombie et al. (2013) where pinewood biochar and paddy husk biochar had respective ash contents of approximately 1%–6% and 37%–50% respectively. The ash content increases with the increasing pyrolysis temperature. This observation has been made in available literature (Crombie et al., 2013; Tomczyk et al., 2020). The high ash content is accompanied by a significant increase in pH_{zpc} in PHBC compared with SDBC at the same pyrolysis temperature.

The fixed matter content of SDBC increases with the increasing temperature. This observation has been made in available literature as well (Crombie et al., 2013; Pariyar et al., 2020). The reason for the increase in the fixed matter content is due to the release of volatiles with the increase in pyrolysis temperature (Crombie et al., 2013). Contrary, the fixed matter content of PHBC reduced with the increase in pyrolysis temperature. This is due to the higher ash content (>20%) of the paddy husk feedstock. Dunnigan et al. (2018), states that an increase in pyrolysis temperature of charring reduces the fixed matter content for feedstocks containing more than 20% ash content. The significant amount of ash in paddy husk which is not liberated during pyrolysis is the reason for this observation (Dunnigan et al., 2018). Comparatively, PHBC had a lower fixed carbon content than SDBC which is due to the lower ash contents on SDBC compared with PHBC (Pariyar et al., 2020).

3.1.3. SEM-EDX analysis of biochar

The SEM images of SDBC synthesized in this study are comparable with the forest wood biochar images (Maljaee et al., 2021). Fig. 2 shows the SEM images of SDBC1 and SDBC2 under 500 × and 5000 × magnification levels. The SDBC contains uneven and randomly distributed cracks and pores. The surface of the PHBC has a rough surface with bulges which have also been observed in past studies (Maljaee et al., 2021). Furthermore, the surface of the sawdust is much coarser than that of paddy husk biochar. The EDX results in Table S.1 show a reduction of oxygen content with an increase in pyrolysis temperature. In SDBC, the oxygen content is significantly lower than in PHBC. This results in SDBC having lower oxygen-containing functional groups than PHBC which are required for heavy metal removal. The increase of Si content in PHBC with pyrolysis temperature increment is due to the higher ash content resulting from the increase in pyrolysis temperature.

3.2. Adsorption results

3.2.1. Effect of initial pH on Cu, Pb and Zn removal by biochar

The pH value of the solution determines the generation of electrons and charged ions on the biochar surface. The initial pH of the solution determines the surface charge of the adsorbent at the start of the removal process. Dissociation of hydroxyl groups and complexation of background electrolyte ions result in the development of the surface electrical charge of an adsorbent (Nasiruddin and Anila, 2007). As H^+ and OH^- ions are potential determining ions, the pH value of the solution determines the generation of electrons and charged ions on the biochar surface (Nasiruddin and Anila, 2007). At pH values lower than the zero-point charge of the adsorbent, the surface of the adsorbent is positive. Also, the functional groups present in biochar are protonated and have a positive charge (Tan et al., 2015). Additionally, H^+ ions

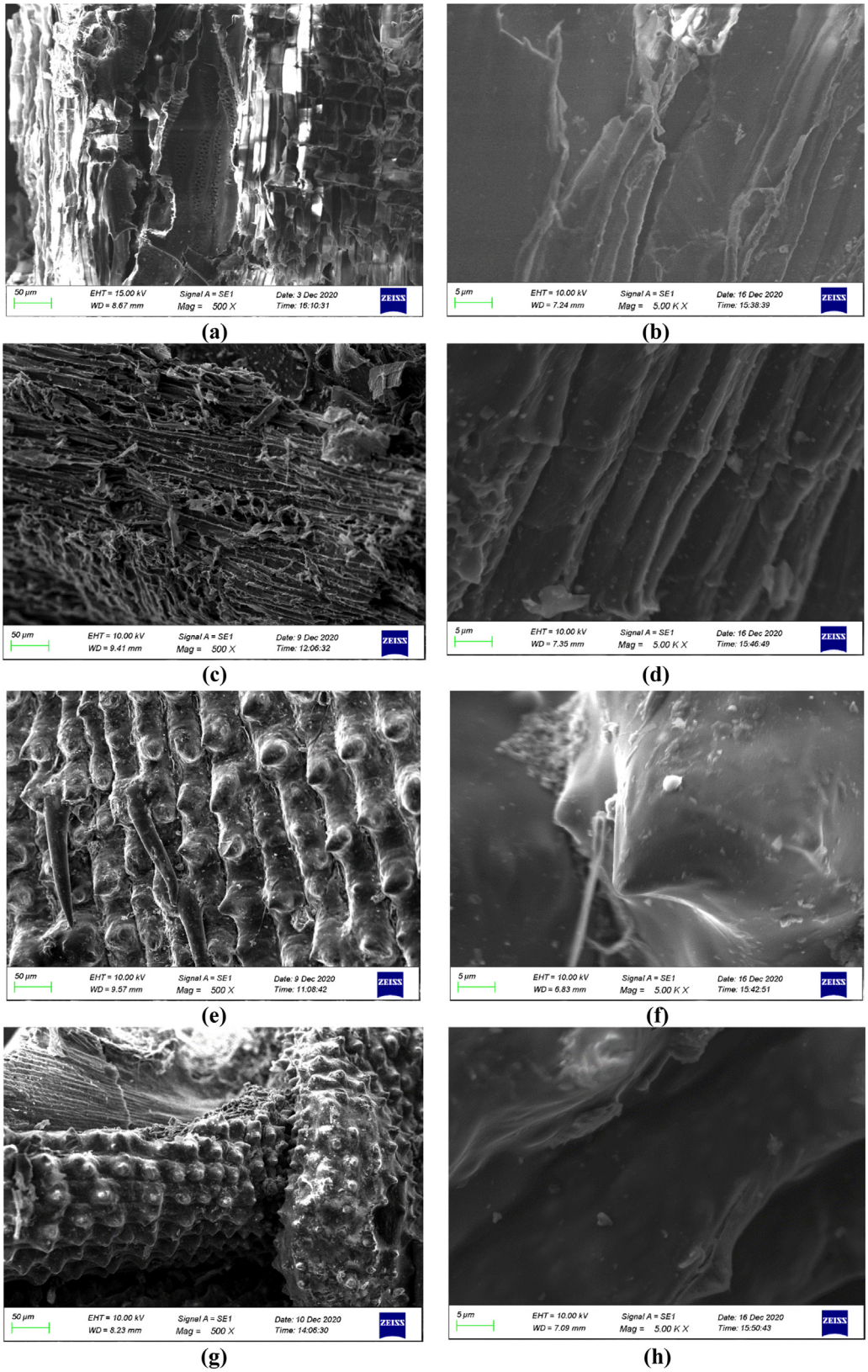

Fig. 2. SEM images of SDBC1 under 500 × magnification (a), SDBC1 under 5000 × magnification (b), SDBC2 under 500 × magnification (c), SDBC2 under 5000 × magnification (d), PHBC1 under 500 × magnification (e), PHBC1 under 5000 × magnification (f), PHBC2 under 500 × magnification (g) and PHBC2 under 5000 × magnification (h).

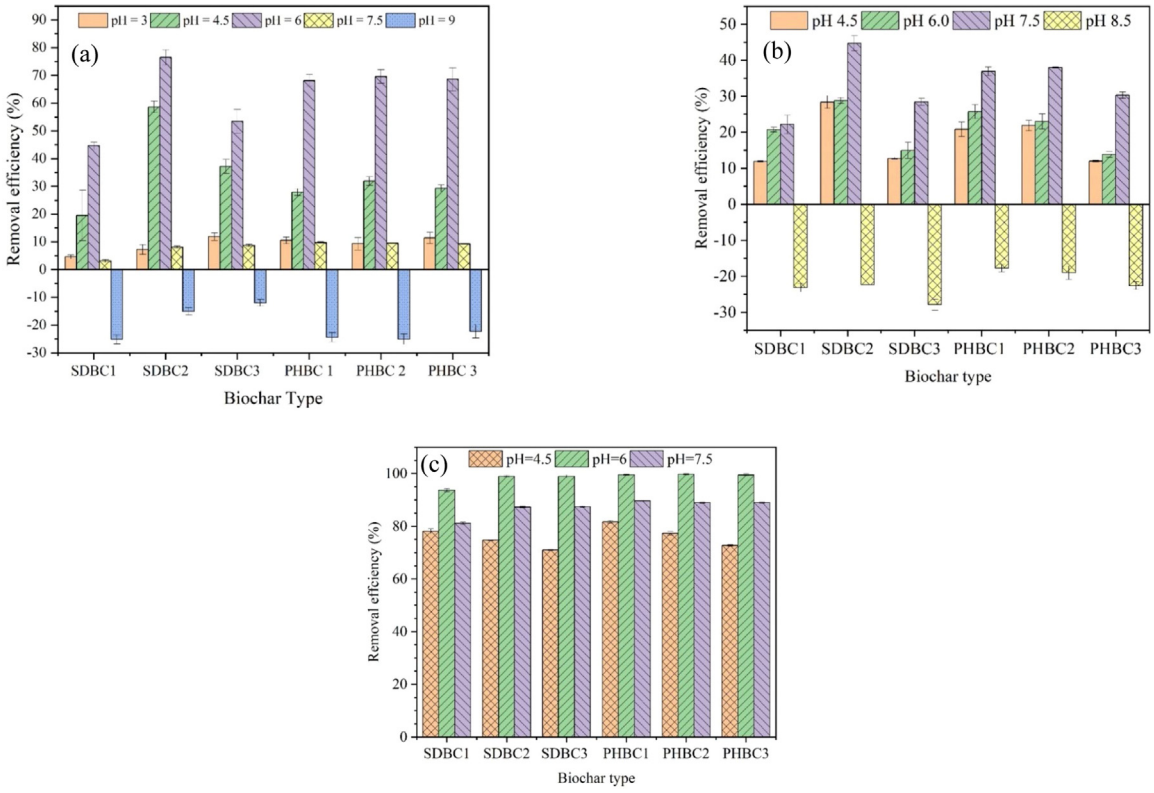

Fig. 3. Variation of Cu (a), Zn (b) and Pb (c) removal with initial pH of the solution for each type of biochar (Temperature = 25 °C; Contact Time = 24 h; Adsorbent dosage = 1 g/L; Initial Cu, Pb and Zn concentration = 10 mg/L).

in the solution induce a competing ion effect on the cations (Tan et al., 2015; Xu et al., 2021). Fig. 3(a)–(c) compares the variation of Cu, Pb and Zn removal with the initial pH of the solution for each type of biochar. A reduction of Cu, Pb and Zn removal efficiencies can be observed at lower pH values (< pH 6). This is due to the surface charge being positive, protonation of functional groups and the competing effect from the H^+ ions at low pH values.

At all initial pH values, SDBC2 shows the optimum removal efficiency for Cu and Zn while also showing removal efficiencies above 99% for Pb. All three PHBCs show a similar removal efficiency for the removal of Cu and Pb for all initial pH values. For Zn removal, PHBC1 and PHBC2 show similar removal efficiencies at an initial pH value of 6. The solubility limit where a minimum of 10 mg/L is soluble corresponds to pH values of 6.24, 6.23 and 7.64 for Cu, Pb and Zn, respectively. The removal efficiencies peak when the initial pH is at the closest value below the solubility limit for the heavy metals. This is closely related to the relative surface charge of the adsorbent. Since the pH_{zpc} values are above the solubility limits, the adsorptive removal best occurs when the positive charge of the surface is at its minimum. Hence, the removal efficiencies peak for Cu and Pb at an initial pH of 6 and the peak removal of Zn is at initial pH equal to 7.5. This is tallying with the range of pH values (5–8) for which the highest removal of Cu, Pb, and Zn is observed (Liu and Zhang, 2009; Shaheen et al., 2018). Another reason is the lowering of the competition of metal ions and protons for binding sites due to the deprotonation of functional groups at higher pH values (Tan et al., 2015). Beyond initial pH values higher than the solubility limits precipitation of the heavy metal hydroxides occurs (Liu and Zhang, 2009; Tan et al., 2015). As the final pH of the solution is less than the initial pH, as shown in Table S2, the concentration of dissolved HMs in the initial solution will be less than that of the final solution resulting in a negative removal efficiency being recorded. A similar change in initial pH has been observed by Chen et al. (2011). The isotherm modeling and kinetic modeling were continued with initial pH values of 6, 6 and 7,5 for Cu, Pb and Zn removal.

3.2.2. Removal mechanisms

The FTIR and XRD spectra of biochar post-adsorption of heavy metals are compared with synthesized biochar to develop an understanding of the mechanisms of the process of removal of heavy metals (Yankovych et al., 2021). For PHBC, the shifting of the peaks is observed at 1566 to 1449 cm^{-1}, 1884 to 1792 cm^{-1}, and 3042 to 2988 cm^{-1}, Figure S3. This suggests that Cu has interacted with the COO–/C=C/C=O (SectionA, Fig. 4), C=O (carboxyl/ester) (Section B, Fig. 4) and O–H (Section D, Fig. 4) functional groups which results in a change in vibration frequency of the bond (Wang et al., 2015). For SDBC, shifting of peaks can be observed for peaks at 1090 cm^{-1}, 1927 cm^{-1} and 3400 cm^{-1}, Figure S6, which

correspond to silanols (Si–OH) and siloxanes (Si–O–Si–OH) groups, C=C=C (allene) and O–H bond groups. Thus, Cu ions have interacted with the Si–OH (Section C, Fig. 4), C=C and O–H (Section D, Fig. 4) functional groups in SDBC. In SDBC2, the peak around 780 cm^{-1} is assigned to b-ring of pyridine, 1600 cm^{-1} is assigned to C=C and C=O acts as a p–donor (Wang et al., 2015; Nguyen et al., 2022). A reduction of the intensity of the peak 780 cm^{-1} and shifting of the peak around 1600 cm^{-1} after the sorption of Cu can be observed. Thus, it can be concluded that the Cu^{+2} + p interaction has occurred during the sorption of Cu by SDBC, shown in section C of Fig. 4 (Wang et al., 2015). In a similar study by Zhou et al. (2018) where tobacco stem biochar was used for Cu removal, interaction with O–H, C=O/C–O and C=O together with Cu^{+2} + p interaction was identified as the mechanisms of Cu^{+2} removal. Zhao et al. (2020) also observed the contribution of Cu^{+2} + p interaction to the adsorptive removal of Cu.

After Pb sorption shift in the peaks of paddy husk biochar was at 1088 cm^{-1}, 1566 cm^{-1}, 2098 cm^{-1}, and 3055 cm^{-1}, Figure S4. This indicates Pb ions have interacted with C–O (Section B, Fig. 4), and –OH or siloxanes (Si–O–Si–OH) (Section B, Fig. 4), COO– or C–C or C=O, C=O of ketones (Section A, Fig. 4) and O–H groups (Section D, Fig. 4) (Wang and Liu, 2017; Mbui et al., 2021). In Figure S7, peak shifting has occurred in the peaks of the silanols (Si–OH)/siloxanes (Si–OO–Si–OH) groups (1090 cm^{-1}) (Section B, Fig. 4), C=C=C (1928 cm^{-1}) (Section A, Fig. 4) and O–H groups (3400 cm^{-1}) (Section D, Fig. 4) suggesting Pb ion interaction with corresponding compounds in SDBC. Further, the shift in CO_3^{2-} (1422 cm^{-1}) (Section D, Fig. 4) peak after Pb adsorption suggests that $PbCO_3$ precipitates have formed. FTIR peaks corresponding to the O–H band in both PHBC and SDBC, C–O and –OH or siloxanes (Si–O–Si–OH) and aromatic C=O bands of carboxylate in SDBC weakened after Pb removal (Zhou et al., 2018). This implies that hydroxyl (Section D, Fig. 4) and carboxyl groups (Section B, Fig. 4) had participated in the storing of Pb^{2+} (Zhou et al., 2018). In SDBC2, the peak around 780 cm^{-1}, assigned to b-ring of pyridine which acts as a p-donor (Wang et al., 2015) shows a reduction of intensity after sorption of Pb. Furthermore, the peak around 1600 cm^{-1} for both PHBC and SDBC assigned to C=C and C=O stretching vibrations is shifted after Pb removal (Wang et al., 2015). Thus, it can be concluded that Pb^{+2} + p interaction (Section C, Fig. 4) is responsible for the sorption of Pb by biochar similar to Cu removal (Wang et al., 2015). Similarly, Zhou et al. (2018) had also noted that functional group complexation, precipitation and Pb^{+2} + p interaction contribute to Pb removal by tobacco stem biochar.

After Zn sorption shifting of peaks of PHBC can be seen at 1566 cm^{-1}, 1885 cm^{-1}, and 3055 cm^{-1} in Figure S5. Thus, Zn ions have interacted with siloxanes (Si–O–Si–OH) (Section B, Fig. 4), C=O of carboxylic (Section B, Fig. 4) and O–H groups (Section D, Fig. 4) of PHBC (Zhao et al., 2019; Mbui et al., 2021). Comparative to PHBC, the interaction of Zn with COO–/C=C/C=O (Section A, Fig. 4), C=O (Carboxyl/Ester) (Section B, Fig. 4) and O–H groups (Section D, Fig. 4) in SDBC can be identified. Comparatively, a higher number of functional groups in SDBC are observed to have interacted in Zn removal. In SDBC2, the peak assigned to b-ring of pyridine shows a reduction of intensity after sorption of Zn, Figure S8. Further, in both PHBC and SDBC, the peak around 1600 cm ^{1}, assigned to C=C and C=O stretching vibration has shifted after Zn removal (Wang et al., 2015). Thus, it can be concluded that Zn^{+2} + p interaction (Section C, Fig. 4) is responsible for the sorption of all three heavy metals including Zn. However, Yankovych et al. (2021) where sunflower biochar was used, only a shift in the C=O bond had been observed and concluded that hydroxyl, carboxylic groups did not participate in Zn removal

Furthermore, the peak around 1400 cm^{-1} is due to the presence of CO_3^{2-} in SDBC which is due to the presence of $CaCO_3$. There is a shift in the peak after adsorption, as seen in Figures S2-7 for Cu, Pb and Zn indicating the possibility of heavy metals being precipitated as carbonates on the surface of biochar (Wang and Liu, 2017). The XRD images in Figure S9 (a)–(f) confirm the presence of the respective carbonates of Cu, Pb and Zn after removal. Precipitation of carbonates was also observed when anaerobically digested biomass biochar was used for Pb removal (Inyang et al., 2012) and when biochar derived from Apple tree branches was used for Cu and Zn removal (Zhao et al., 2020). The broad peak of –OH appearing around 3000–3400 cm^{-1} in both biochar materials has shifted after adsorption of Cu, Pb and Zn, suggesting the interaction of the three heavy metals with the –OH functional group. This indicated the possibility of surface complexation of Cu, Pb and Zn with –OH (Xue et al., 2020; Xu et al., 2021). The presence of Cu, Pb and Zn hydroxides in both PHBC and SDBC after adsorption can be observed in XRD images of Figure S9 (a)–(f) which is shown in section D of Fig. 4. Deng et al. (2021) and Lian et al. (2021) had made similar observations using Magnesium modified biochar and Oyster shell waste biochar. Thus, heavy metals are removed due to several mechanisms ranging from ion exchange to physical adsorption and the common mechanisms are shown in Fig. 4.

3.2.3. Effect of contact time on Cu, Pb and Zn removal by PHBC1 and SDBC2

A comparison of Cu, Pb and Zn removal variation with the contact time of the solution for each type of biochar is shown in Figure S10. Both the SDBC and PHBC adsorbents showed similar equilibrium contact times for the same pollutant. The equilibrium contact time primarily depends on the type of heavy metal rather than the adsorbent material. The availability of an adequate number of binding sites in both types of adsorbents is hypothesized as the reason for this observation. However, this is different from the observation made by Zhao et al. (2019) where the contact times for Cu, Pb, Cr and Cd changed as the feedstock type of biochar changed.

The rate of metal sorption is assumed to be proportional to the number of unoccupied sites in Pseudo First order and Pseudo Second-order models. Table 2 shows the summary of correlation efficiencies R^2 for Pseudo First-rate order and Pseudo Second-rate order models. The pseudo-Second-order model best fits the adsorption data. The Pseudo-Second-order model has previously been selected to best describe heavy metal adsorption by biochar made from sunflower (Yankovych

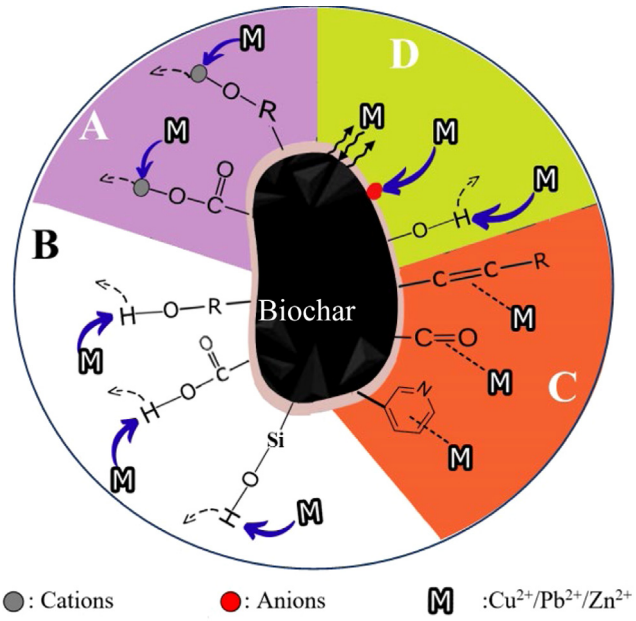

Fig. 4. Mechanisms of HM removal from synthesized biochar (A: Ion Exchange, B: Surface complexation, C: p-electron interactions, D: Physical adsorption, Co-precipitation, Surface precipitation).

Table 2
Adsorption kinetic modeling for Cu, Pb and Zn adsorption by biochar materials.

Biochar type	Cu		Pb		Zn	
	First-order-rate constants	Second-order-rate constants	First-order-rate constants	Second-order-rate constants	First-order-rate constants	Second-order-rate constants
SDBC2	0.8818	0.9755	0.9552	0.9985	0.8486	0.9984
PHBC1	0.8207	0.9477	0.9691	0.9995	0.7483	0.9965

et al., 2021), Paper Mill Sludge (Xu et al., 2021), Oyster Shell waste (Lian et al., 2021), Apple Tree Branches (Zhao et al., 2020) and Poultry Manure (Batool et al., 2017). Hence, the sorption of all three heavy metals by the PHBC and SDBC is mainly via chemisorption, which involves electrostatic attraction, ion exchange, complexation and precipitation between the active sites of the adsorbent (Deng et al., 2021; Xu et al., 2021). Table S3 summarizes the model parameters for the Pseudo Second-order model. The adsorption rate constant can be used to idealize the speed of adsorption of an adsorbate to an adsorbent (Chen et al., 2011). From the adsorption rate constants, Cu adsorbs onto SDBC quicker than to PHBC despite the higher adsorption capacity of PHBC with respect to Cu removal. A similar result was observed by Chen et al. (2011) where the Cu adsorption rate was higher in the adsorbent with comparatively lower adsorption capacity. On the other hand, Pb and Zn are adsorbed faster on PHBC than SDBC.

3.2.4. Isotherm analysis of SDBC2 and PHBC1

Isotherm modeling enables the evaluation of the most suitable theoretical adsorption method (monolayer or multi-layer adsorption). Results of adsorption isotherm modeling for Cu, Pb and Zn adsorption by biochar materials are given in Table 3. The Langmuir monolayer isotherm best describes the removal of all three heavy metals which is consistent with past studies using biochar for heavy metal removal (Shen et al., 2017; Lian et al., 2021; Xu et al., 2021). The R_L value, a dimensionless constant separation factor is used to describe the effectiveness of the adsorption. It is calculated using the ratio of unused adsorption capacity to the maximum adsorption capacity. For the initial concentration of 10 mg/L of all three heavy metals, the R_L value is between 0 and 1 which implies favorable adsorption (Mohan et al., 2007). Parameter b which is related to the affinity of the binding sites provides an understanding of the affinity of biochar towards heavy metal ions (Chen et al., 2011). The values of parameter b for Cu, Pb and Zn removal by SDBC are 6.661, 0.734, 0.741 l/mg, respectively. For PHBC these are 0.994, 1.191 and 0.171 l/mg. Thus, Cu and Zn are observed to have a higher affinity towards SDBC while Pb has a higher affinity towards PHBC. The maximum adsorption capacities of the PHBC and SDBC are similar to those reported found in previous similar studies. Table S4 gives a summary of adsorption capacities observed in the published literature.

Table 3
Adsorption isotherm modeling for Cu, Pb and Zn adsorption by biochar materials.

Biochar type	Cu						Pb						Zn					
	Langmuir			Freundlich			Langmuir			Freundlich			Langmuir			Freundlich		
	q_{max} (mg/g)	R_L	Correlation factor	k_f (mg/g)	n	Correlation factor	q_{max} (mg/g)	R_L	Correlation factor	k_f (mg/g)	n	Correlation factor	q_{max} (mg/g)	R_L	Correlation factor	k_f (mg/g)	n	Correlation factor
SDBC2	6.89	0.0148	0.9444	5.55	9.40	0.0857	17.57	0.1199	0.8825	9.96	6.89	0.2229	2.64	0.1189	0.8713	5.54	−6.89	0.2261
PHBC1	10.27	0.0914	0.9778	5.87	4.65	0.7804	14.20	0.0774	0.8854	9.20	9.42	0.2289	6.48	0.3683	0.9146	1.45	2.19	0.8808

4. Conclusions

The effect of pyrolysis temperature on sawdust biochar was more significant (∼50%) than paddy husk biochar for the removal of Cu and Zn due to the significant lowering of the functional groups in SDBC with an increase in pyrolysis temperature. However, no significant (<10%) effect of either feedstock or pyrolysis temperature was observed on Pb removal. The optimum pH values of removal observed for all three heavy metals were higher than the zero-point charge of the adsorbents suggesting that the physical attraction of the heavy metals to the surface was insignificant compared to chemical attraction. The higher intensity of the FTIR peaks of PHBC compared to SDBC suggested that PHBC has a greater volume of functional groups compared to SDBC. Pseudo-second order model best-fitted adsorption kinetics and the Langmuir monolayer isotherm best described the removal of all three heavy metals. The maximum adsorption capacities of Cu and Zn were 10.27 and 6.48 mg/g was achieved with PHBC while the maximum Pb adsorption capacity of 17.57 mg/g was achieved by SDBC suggesting that removal of Cu and Zn was more dependent upon interactions with the surface with functional groups than Pb. Surface complexation, co-precipitation, *p*- electron interactions, physical adsorption and surface precipitation were identified as the main mechanisms of removal of the three heavy metals. Therefore, the results of this study show promising evidence of new prospects for biochar synthesis and in using industrially manufactured biochar for stormwater treatment.

CRediT authorship contribution statement

Pamodithya Wijeyawardana: Conceptualization, Data curation, Experiment, Formal analysis, Investigation, Methodology, Validation, Writing – original draft. **Nadeeshani Nanayakkara:** Conceptualization, Supervision, Writing – review & editing. **Chamila Gunasekara:** Conceptualization, Supervision, Writing – review & editing. **Anurudda Karunarathna:** Conceptualization, Supervision, Writing – review & editing. **David Law:** Conceptualization, Supervision, Writing – review & editing. **Biplob Kumar Pramanik:** Conceptualization, Project administration, Supervision, Writing – review & editing.

Declaration of competing interest

The authors declare that they have no known competing financial interests or personal relationships that could have appeared to influence the work reported in this paper.

Acknowledgment

Scholarship provided by the School of Engineering, RMIT University and University of Peradeniya Research Grant URG/2021/19/E, are gratefully acknowledged.

Appendix A. Supplementary data

Supplementary material related to this article can be found online at https://doi.org/10.1016/j.eti.2022.102640.

References

Alahakoon, A.M.Y.W., Karunarathna, A.K., Dharmakeerthi, R.S., 2018. Performance evaluation of a down draft double chamber pyrolysis reactor under field conditions. Trop. Agric. Res. 30, 84–94.

Alhashimi, Hashim A., Aktas, Can B, 2017. Life cycle environmental and economic performance of biochar compared with activated carbon: A meta-analysis. Resour. Conserv. Recy. 118, 13–26.

Batool, S., Idrees, M., Hussain, Q., Kong, J., 2017. Adsorption of copper (II) by using derived-farmyard and poultry manure biochars: Efficiency and mechanism. Chem. Phys. Lett. 689, 190–198.

Chen, X., Chen, G., Chen, L., Chen, Y., Lehmann, J., Mcbride, M.B., Hay, A.G., 2011. Adsorption of copper and zinc by biochars produced from pyrolysis of hardwood and corn straw in aqueous solution. Bioresour. Technol. 102, 8877–8884.

Chen, Xiao, Niu, Zidong, Zhang, Haoyu, Lu, Mingyu, Lu, Yalei, Zhou, Mingkai, Li, Beixing, 2020. Design of a chitosan modifying alkali-activated slag pervious concrete with the function of water purification. Constr. Build. Mater. 251, 118979.

Crombie, K., Mašek, O., Sohi, S.P., Brownsort, P., Cross, A., 2013. The effect of pyrolysis conditions on biochar stability as determined by three methods. GCB Bioenergy 5, 122–131.

Dai, Y., Zhang, N., Xing, C., Cui, Q., Sun, Q., 2019. The adsorption, regeneration and engineering applications of biochar for removal organic pollutants: A review. Chemosphere 223, 12–27.
Deng, Y., Li, X., Ni, F., Liu, Q., Yang, Y., Wang, M., Ao, T., Chen, W., 2021. Synthesis of magnesium modified biochar for removing copper, lead and cadmium in single and binary systems from aqueous solutions: Adsorption mechanism. Water 13.
Dunnigan, L., Ashman, P.J., Zhang, X., Kwong, C.W., 2018. Production of biochar from rice husk: Particulate emissions from the combustion of raw pyrolysis volatiles. J. Clean. Prod. 172, 1639–1645.
Duruibe, J.O., Ogwuegbu, M.O.C., Egwurugwu, J.N., 2007. Heavy metal pollution and human biotoxic effects. Int. J. Phys. Sci. 2, 112–118.
Efome, J.E., Rana, D., Matsuura, T., Lan, C.Q., 2018a. Experiment and modeling for flux and permeate concentration of heavy metal ion in adsorptive membrane filtration using a metal–organic framework incorporated nanofibrous membrane. Chem. Eng. J. 352, 737–744.
Efome, J.E., Rana, D., Matsuura, T., Lan, C.Q., 2018b. Insight studies on metal–organic framework nanofibrous membrane adsorption and activation for heavy metal ions removal from aqueous solution. ACS Appl. Mater. Interfaces 10, 18619–18629.
Efome, J.E., Rana, D., Matsuura, T., Lan, C.Q., 2018c. Metal–organic frameworks supported on nanofibers to remove heavy metals. J. Mater. Chem. A 6, 4550–4555.
Engwa, G.A., Ferdinand, P.U., Nwalo, F.N., Unachukw, M.N., 2018. Mechanism and health effects of heavy metal toxicity in humans. In: Poisoning in the Modern World - New Tricks for an Old Dog?.
Feola Conz, R., Abbruzzini, T.F., De Andrade, C.A., Milori, D.M.B.P., Cerri, C.E.P., 2017. Effect of pyrolysis temperature and feedstock type on agricultural properties and stability of biochars. Agric. Sci. 08, 914–933.
Gu, S., Boase, E.M., Lan, C.Q., 2021. Enhanced Pb(II) removal by green alga neochloris oleoabundans cultivated in high dissolved inorganic carbon cultures. Chem. Eng. J. 416.
Heredia Salgado, M.A., Coba, S.J.A., Tarelho, L.A.C., 2020. Simultaneous production of biochar and thermal energy using palm oil residual biomass as feedstock in an auto-thermal prototype reactor. J. Clean. Prod. 266.
Hodgson, E., Lewys-James, A., Rao Ravella, S., Thomas-Jones, S., Perkins, W., Gallagher, J., 2016. Optimisation of slow-pyrolysis process conditions to maximise char yield and heavy metal adsorption of biochar produced from different feedstocks. Bioresour. Technol. 214, 574–581.
Inyang, M.I., Gao, B., Yao, Y., Xue, Y., Zimmerman, A., Mosa, A., Pullammanappallil, P., Ok, Y.S., Cao, X., 2015. A review of biochar as a low-cost adsorbent for aqueous heavy metal removal. Crit. Rev. Environ. Sci. Technol. 46, 406–433.
Inyang, M., Gao, B., Yao, Y., Xue, Y., Zimmerman, A.R., Pullammanappallil, P., Cao, X., 2012. Removal of heavy metals from aqueous solution by biochars derived from anaerobically digested biomass. Bioresour. Technol. 110, 50–56.
Kayhanian, M., Stransky, C., Bay, S., Lau, S.L., Stenstrom, M.K., 2008. Toxicity of urban highway runoff with respect to storm duration. Sci. Total Environ. 389, 386–406.
Kumar, P.S., Gayathri, R., Rathi, B.S., 2021. A review on adsorptive separation of toxic metals from aquatic system using biochar produced from agro-waste. Chemosphere 285, 131438.
Lago, B.C., Silva, C.A., Melo, L.C.A., Morais, E.G., 2021. Predicting biochar cation exchange capacity using Fourier transform infrared spectroscopy combined with partial least square regression. Sci. Total Environ. 794, 148762.
Lian, W., Li, H., Yang, J., Joseph, S., Bian, R., Liu, X., Zheng, J., Drosos, M., Zhang, X., Li, L., Shan, S., Pan, G., 2021. Influence of pyrolysis temperature on the cadmium and lead removal behavior of biochar derived from oyster shell waste. Bioresour. Technol. Rep. 15.
Lin, T.-Y., Kuo, C.-P., 2012. Study of products yield of bagasse and sawdust via slow pyrolysis and iron-catalyze. J. Analytical Appl. Pyrolysis 96, 203–209.
Liu, Z., Zhang, F.S., 2009. Removal of lead from water using biochars prepared from hydrothermal liquefaction of biomass. J. Hazard Mater. 167, 933–939.
Ma, Y., Egodawatta, P., Mcgree, J., Liu, A., Goonetilleke, A., 2016. Human health risk assessment of heavy metals in urban stormwater. Sci. Total Environ. 557–558, 764–772.
Maljaee, H., Paiva, H., Madadi, R., Tarelho, L.A.C., Morais, M., Ferreira, V.M., 2021. Effect of cement partial substitution by waste-based biochar in mortars properties. Construct. Build. Mater. 301.
Mbui, D., Njomo, N., Gitita, M., Ndekei, A., 2021. Synthesis and characterization of rice husk biochar and its application in the adsorption studies of lead and copper. Int. Res. J. Pure Appl. Chem. 3, 6–50.
Mohan, D., Pittman Jr., C.U., Bricka, M., Smith, F., Yancey, B., Mohammad, J., Steele, P.H., Alexandre-Franco, M.F., Gomez-Serrano, V., Gong, H., 2007. Sorption of arsenic, cadmium, and lead by chars produced from fast pyrolysis of wood and bark during bio-oil production. J. Colloid Interface Sci. 310, 57–73.
Mullaney, J., Lucke, T., 2014. Practical review of pervious pavement designs. CLEAN - Soil, Air, Water 42 (2), 111–124.
Nasiruddin, M.K., Anila, S., 2007. Determination of points of zero charge of natural and treated adsorbents. Surf. Rev. Lett. 14, 461–469.
Nguyen, T.D., Nguyen, T.M.P., Van, H.T., Nguyen, V.Q., Nguyen, L.H., Nguyen, T.D., Nguyen, T.H.V., Chu, T.H.H., Nguyen, T.H., Ha, L.T., Vinh, N.D., Thai, V.N., Nguyen, V.Q., Nguyen, K.A., Thang, P.Q., 2022. Adsorption removal of ammonium from aqueous solution using Mg/Al layered double hydroxides-zeolite composite. Environ. Technol. Innov. 25.
Pariyar, P., Kumari, K., Jain, M.K., Jadhao, P.S., 2020. Evaluation of change in biochar properties derived from different feedstock and pyrolysis temperature for environmental and agricultural application. Sci. Total Environ. 713, 136433.
Park, J.-H., Wang, J.J., Kim, S.-H., Cho, J.-S., Kang, S.-W., Delaune, R.D., Han, K.-J., Seo, D.-C., 2017. Recycling of rice straw through pyrolysis and its adsorption behaviors for Cu and Zn ions in aqueous solution. Colloids Surf. A 533, 330–337.
Poo, K.-M., Son, E.-B., Chang, J.-S., Ren, X., Choi, Y.-J., Chae, K.-J., 2018. Biochars derived from wasted marine macro-algae (saccharina japonica and sargassum fusiforme) and their potential for heavy metal removal in aqueous solution. J. Environ. Manag. 206, 364–372.
Reddy, K.R., Xie, T., Dastgheibi, S., 2014. Removal of heavy metals from urban stormwater runoff using different filter materials. J. Environ. Chem. Eng. 2, 282–292.
Sakson, G., Brzezinska, A., Zawilski, M., 2018. Emission of heavy metals from an urban catchment into receiving water and possibility of its limitation on the example of lodz city. Environ. Monit. Assess. 190 (281).
Saleh, T.A., 2015. Nanocomposite of carbon nanotubes/silica nanoparticles and their use for adsorption of Pb(II): from surface properties to sorption mechanism. Desalin. Water Treat. 57, 10730–10744.
Shaheen, S.M., Niazi, N.K., Hassan, N.E.E., Bibi, I., Wang, H., Tsang, C.W., Ok, Y.S., Bolan, N., Rinklebe, J., 2018. Wood-based biochar for the removal of potentially toxic elements in water and wastewater: a critical review. Int. Mater. Rev. 64, 216–247.
Shen, Z., Zhang, Y., Jin, F., Mcmillan, O., Al-Tabbaa, A., 2017. Qualitative and quantitative characterisation of adsorption mechanisms of lead on four biochars. Sci. Total Environ. 609, 1401–1410.
Sidhu, V., Barrett, K., Park, D.Y., Deng, Y., Datta, R., Sarkar, D., 2020. Wood mulch coated with iron-based water treatment residuals for the abatement of metals and phosphorus in simulated stormwater runoff. Environ. Technol. Innov..
Soni, B., Karmee, S.K., 2020. Towards a continuous pilot scale pyrolysis based biorefinery for production of biooil and biochar from sawdust. Fuel 271.
Sun, C., Chen, T., Huang, Q., Wang, J., Lu, S., Yan, J., 2019. Enhanced adsorption for Pb(II) and Cd(II) of magnetic rice husk biochar by KMnO4 modification. Environ. Sci. Pollut. Res. Int. 26, 8902–8913.

Tan, X., Liu, Y., Zeng, G., Wang, X., Hu, X., Gu, Y., Yang, Z., 2015. Application of biochar for the removal of pollutants from aqueous solutions. Chemosphere 125, 70–85.
Tchounwou, P.B., Yedjou, C.G., Patlolla, A.K., Sutton, D.J., 2012. Heavy metal toxicity and the environment. In: Molecular, Clinical and Environmental Toxicology. In: Experientia Supplementum, 101, Springer, Basel, pp. 133–164.
Tomczyk, A., Sokołowska, Z., Boguta, P., 2020. Biochar physicochemical properties: pyrolysis temperature and feedstock kind effects. Rev. Environ. Sci. Bio/Technol. 19, 191–215.
Tripathi, M., Sahu, J.N., Ganesan, P., 2016. Effect of process parameters on production of biochar from biomass waste through pyrolysis: A review. Renew. Sustain. Energy Rev. 55, 467–481.
USEPA, 2014. National Recommended Water Quality Criteria Tables [Online]. Office of Science and Technology, Available, Accessed2nd,2021.
Štefelová, J., Zelenka, T., Slovák, V., 2017. Biosorption (removing) of Cd(II), Cu(II) and methylene blue using biochar produced by different pyrolysis conditions of beech and spruce sawdust. Wood Sci. Technol. 51, 1321–1338.
Wang, Y., Liu, R., 2017. Comparison of characteristics of twenty-one types of biochar and their ability to remove multi-heavy metals and methylene blue in solution. Fuel Process. Technol. 160, 55–63.
Wang, Z., Liu, G., Zheng, H., Li, F., Ngo, H.H., Guo, W., Liu, C., Chen, L., Xing, B., 2015. Investigating the mechanisms of biochar's removal of lead from solution. Bioresour. Technol. 177, 308–317.
Wijeyawardana, P., Nanayakkara, N., Gunasekara, C., Karunarathna, A., Law, D., Pramanik, B.K., 2022. Improvement of heavy metal removal from urban runoff using modified pervious concrete. Sci. Total Environ. 815, 152936.
Williams, P.T., S, B., 1996. The influence of temperature and heating rate on the slow pyrolysis of biomass. Renew. Energy 7, 233–250.
Xu, Z., Lin, Y., Lin, Y., Yang, D., Zheng, H., 2021. Adsorption behaviors of paper mill sludge biochar to remove Cu, Zn and As in wastewater. Environ. Technol. Innov. 23.
Xue, C., Zhu, L., Lei, S., Liu, M., Hong, C., Che, L., Wang, J., Qiu, Y., 2020. Lead competition alters the zinc adsorption mechanism on animal-derived biochar. Sci. Total Environ. 713, 136395.
Yankovych, H., Novoseltseva, V., Kovalenko, O., Behunova, D.Marcin., Kanuchova, M., Vaclavikova, M., Melnyk, I., 2021. New perception of Zn(II) and Mn(II) removal mechanism on sustainable sunflower biochar from alkaline batteries contaminated water. J. Environ. Manage. 292, 112757.
Zhao, J., Shen, X.J., Domene, X., Alcaniz, J.M., Liao, X., Palet, C., 2019. Comparison of biochars derived from different types of feedstock and their potential for heavy metal removal in multiple-metal solutions. Sci. Rep. 9 (9869).
Zhao, S., Ta, N., Wang, X., 2020. Absorption of cu(II) and Zn(II) from aqueous solutions onto biochars derived from apple tree branches. Energies 13.
Zhou, Y., Liu, X., Xiang, Y., Wang, P., Zhang, J., Zhang, F., Wei, J., Luo, L., Lei, M., Tang, L., 2017. Modification of biochar derived from sawdust and its application in removal of tetracycline and copper from aqueous solution: Adsorption mechanism and modelling. Bioresour. Technol. 245, 266–273.
Zhou, Z., Xu, Z., Feng, Q., Yao, D., Yu, J., Wang, D., Lv, S., Liu, Y., Zhou, N., Zhong, M.-E., 2018. Effect of pyrolysis condition on the adsorption mechanism of lead, cadmium and copper on tobacco stem biochar. J. Clean. Prod. 187, 996–1005.
Zuraini, N.A., Alias, N., Mohamed Yusof, Z., Hanapi, M.N., Harun, S., 2018. First flush analysis of urban stormwater runoff from an urban catchment in Johor, Malaysia, MATEC Web of Conferences 250, 06014.